RESEARCH ARTICLE

Single-cell transcriptome atlas reveals protective characteristics of COVID-19 mRNA vaccine

Yong Tan[1,2] | Shuaiyao Lu[3] | Bo Wang[1] | Xuewen Duan[1] | Yunkai Zhang[4,5] | Xiaozhong Peng[3] | Hangwen Li[6] | Ang Lin[7] | Zhenzhen Zhan[1,2] | Xingguang Liu[4,5]

[1]Research Center for Translational Medicine, Shanghai East Hospital, Tongji University School of Medicine, Shanghai, China

[2]Department of Liver Surgery, Shanghai Institute of Transplantation, Renji Hospital, Shanghai Jiao Tong University School of Medicine, Shanghai, China

[3]National Kunming High-level Biosafety Primate Research Center, Institute of Medical Biology, Chinese Academy of Medical Sciences and Peking Union Medical College, Yunnan, China

[4]Department of Pathogen Biology, Naval Medical University, Shanghai, China

[5]National Key Laboratory of Medical Immunology, Naval Medical University, Shanghai, China

[6]Stemirna Therapeutics, Shanghai, China

[7]Vaccine Center, School of Basic Medicine and Clinical Pharmacy, China Pharmaceutical University, Nanjing, China

Correspondence
Xingguang Liu, Department of Pathogen Biology, Naval Medical University, Shanghai, China.
Email: liuxg@immunol.org

Zhenzhen Zhan, Research Center for Translational Medicine, Shanghai East Hospital, Tongji University School of Medicine, Shanghai, China.
Email: zhanzz@tongji.edu.cn

Ang Lin, Vaccine Center, School of Basic Medicine and Clinical Pharmacy, China Pharmaceutical University, Nanjing, China.
Email: anglin@cpu.edu.cn

Abstract

Messenger RNA (mRNA) vaccines are promising alternatives to conventional vaccines in many aspects. We previously developed a lipopolyplex (LPP)-based mRNA vaccine (SW0123) that demonstrated robust immunogenicity and strong protective capacity against severe acute respiratory syndrome coronavirus-2 (SARS-CoV-2) infection in mice and rhesus macaques. However, the immune profiles and mechanisms of pulmonary protection induced by SW0123 remain unclear. Through high-resolution single-cell analysis, we found that SW0123 vaccination effectively suppressed SARS-CoV-2-induced inflammatory responses by inhibiting the recruitment of proinflammatory macrophages and increasing the frequency of polymorphonuclear myeloid-derived suppressor cells. In addition, the apoptotic process in both lung epithelial and endothelial cells was significantly inhibited, which was proposed to be one major mechanism contributing to vaccine-induced lung protection. Cell−cell interaction in the lung compartment was also altered by vaccination. These data collectively unravel the mechanisms by which the SW0123 protects against lung damage caused by SARS-CoV-2 infection.

KEYWORDS
inflammatory responses, lung protection, mRNA vaccine, polymorphonuclear myeloid-derived suppressor cells (PMN-MDSCs), SARS-CoV-2

Yong Tan, Shuaiyao Lu and Bo Wang are contributed equally to this study.

1 | INTRODUCTION

The pandemic of the ongoing coronavirus disease 2019 (COVID-19) has seriously threatened the public health. Patients with severe COVID-19 normally present acute respiratory distress syndrome, which leads to respiratory failure that causes 70% of COVID-19-related death.[1] In addition, severe infection is largely accompanied by the production of large amounts of cytokines that causes "cytokine storm" or even sepsis symptoms, which is also one leading cause of COVID-19 deaths.[1]

Messenger RNA (mRNA) vaccine technology is based on a lipid-based delivery system that delivers mRNAs encoding immunogens to target cells, thereby allowing the host cells to produce the target antigens to elicit specific vaccine responses. BNT162b2 (BioNTech) and mRNA-1273 (Moderna) are the only two COVID-19 mRNA vaccines authorized by World Health Organization for human use, and both show robust immunogenicity and strong protective efficacy. We have previously developed a novel COVID-19 mRNA vaccine (SW0123) using our proprietary lipopolyplex which showed robust immunogenicity and strong protective efficacy. Extensive evaluations of SW0123 in mouse and nonhuman primate models showed that SW0123 was highly immunogenic to elicit efficient protection against severe acute respiratory syndrome coronavirus-2(SARS-CoV-2) infection.[2] However, we still lack knowledge of how SW0123 vaccination shapes the immune profiles of the lung following SARS-CoV-2 infection and how these changes are associated with protective responses at a single-cell level. To address this, lung specimens from rhesus macaques that had been fully immunized with SW0123 or phosphate buffered saline (PBS) followed by SARS-CoV-2 infection were collected and subjected to single-cell transcriptomic analysis.

We found that SW0123 vaccination effectively suppressed the inflammatory response by reducing the recruitment of proinflammatory macrophages and increasing the proportion of polymorphonuclear myeloid-derived suppressor cells (PMN-MDSCs) post-SARS-CoV-2 infection. Moreover, cell apoptosis-associated gene signatures of both lung epithelial and endothelial cells were significantly altered, suggesting that SW0123 vaccination reduced the susceptibility of lung structural cells to SARS-CoV-2 infection. In addition, SW0123 vaccination altered the single-cell landscape and cell−cell interactions in the lung compartment, including alveolar type 2 (AT2) cell−alveolar type 1 (AT1) cell interaction and AT2 cell−macrophage interaction. Some ligand−receptor interactions, such as laminin subunit beta 2 (LAMB2)−([integrin subunit alpha 1 [ITGA1] + integrin subunit beta 1 [ITGB1]) and collagen type IV alpha 2 chain (COL4A2)−syndecan 4 (SDC4), were significantly enhanced, which might be one of the mechanisms contributing to the protective capacity of SW0123.

2 | MATERIALS AND METHODS

2.1 | Vaccination and SARS-CoV-2 challenge

As previously reported,[2] rhesus macaques (4 years old, male) were intramuscularly immunized with 200 μg SW0123 at Day 0, Day 14, and Day 33 in a volume of 100 μl. Two weeks after the third SW0123 vaccination, rhesus macaques were anesthetized and then challenged intranasally and intratracheally with 1×10^6 plaque formation unit of SARS-CoV-2 (Wuhan/IVDC-HB-01/2019). At Day 7 postinfection, rhesus macaques were anesthetized and necropsied. Bronchoalveolar lavage fluid (BALF), and lung tissues from upper, middle, and lower lobes of left or right lungs were collected. Chinese rhesus macaques were provided and housed in National Kunming High-level Biosafety Primate Research Center, China. All experiments with live SARS-CoV-2 in rhesus macaque model were conducted in ABSL-4 facility. All animal studies were approved by local ethics committees and performed according to the ethical regulations.

2.2 | Lung pathology scoring

The pathological sections of each lung lobe from rhesus macaques were rated, and the scores referred to the main pathological features of COVID-19 patients: the degree of septal thickening or solidity, the degree of septal hemorrhage, the degree of inflammatory cell infiltration, vascular thrombosis, the area of dust cell distribution and other characteristic indicators were rated via relative quantitation. The score for each indicator was determined on a scale of 1−5 depending on the degree of pathology, and the sum of the above scores was the pathology score of one field of view. Each lung lobe of each rhesus macaque was first scanned in full image and the pathological distribution was evaluated comprehensively, at least five fields of view were selected for scoring. The average of all scores from six lung lobes of a rhesus macaque was the result of the overall pathological score, and then was statistically compared with the control group.

2.3 | Hematoxylin and eosin (HE) staining

The samples were harvested and fixed in formaldehyde, dehydrated, embedded in paraffin, and sectioned. After deparaffinization and rehydration, tissue sections were stained with hematoxylin solution for 5 min and soaked in 1% acid ethanol (1% HCl in 75% ethanol). Then the sections were stained with eosin solution for 3 min, followed by dehydration with graded alcohol and clearing in xylene.

2.4 | Immunostaining and terminal deoxynucleotidyl transferase-mediated 2'-deoxyuridine 5'-triphosphate (dUTP) nick-end labeling (TUNEL) assay

TUNEL was assessed with tetramethylrhodamine (TMR) Red In Situ Death Detection Kit (Roche Diagnostics) according to the manufacturer's instructions. Briefly, paraffin-embedded tissue sections were treated with dewaxation rehydration protease. Then, tissue sections were permeabilized and incubated with anti-CD31 antibody

(proteintech) at 4°C overnight. Alexa-Fluor-594-conjugated secondary antibodies (Invitrogen) were incubated at room temperature for 60 min in the dark. Then these sections were incubated with a TUNEL reaction mixture for 60 min. Slices were mounted with a 4', 6'-diamidino-2-phenylindole-containing medium, and fluorescence was observed with an inverted fluorescence microscope (Leica).

2.5 | Tissue dissociation and cell purification

Tissues were transported in sterile culture dish with 10 ml Dulbecco's Phosphate-Buffered Saline (DPBS; Thermo Fisher Scientific) on ice to remove the residual tissue storage solution, then minced on ice. We used dissociation enzyme collagenase IV dissolved in PBS to digest the tissues. Lung tissues were dissociated at 37°C with a shaking speed of 50 rpm for about 40 min. The dissociated cells were repeatedly collected at interval of 20 min to increase cell yield and viability. Cell suspensions were filtered using a 40 μm nylon cell strainer and red blood cells were removed by Red Blood Cell Lysis Solution (Thermo Fisher Scientific). Dissociated cells were washed three times with DPBS. Cells were stained with 0.4% Trypan blue (Thermo Fisher Scientific) to check the viability on Countess II Automated Cell Counter (Thermo Fisher Scientific). The extracted single cells were further subjected to single-cell transcriptomic analysis.

2.6 | 10× library preparation and sequencing

Beads with unique molecular identifier (UMI) and cell barcodes were loaded close to saturation, so that each cell was paired with a bead in a Gel Beads-in-emulsion. After exposure to cell lysis buffer, polyadenylated RNA molecules hybridized to the beads. Beads were retrieved into a single tube for reverse transcription. On complementary DNA (cDNA) synthesis, each cDNA molecule was tagged on the 5′ end with UMI and cell label indicating its cell of origin. Briefly, 10× beads that were then subject to second-strand cDNA synthesis, adapter ligation, and universal amplification. Sequencing libraries were prepared using randomly interrupted whole-transcriptome amplification products to enrich the 3′ end of the transcripts linked with the cell barcode and UMI. All the remaining procedures including the library construction were performed according to the standard manufacturer's protocol (CG000206 Rev D). Sequencing libraries were quantified using a High Sensitivity DNA Chip (Agilent) on a Bioanalyzer 2100 and the Qubit High Sensitivity DNA Assay (Thermo Fisher Scientific). The libraries were sequenced on NovaSeq6000 (Illumina) using 2 × 150 chemistry.

2.7 | Single-cell RNA sequencing (scRNA-seq) data processing

For the 10× data, the Cell Ranger Single-Cell toolkit (version 3.0.0) provided by 10× Genomics was applied to align reads and generate the gene–cell UMI matrix for each sample. Different samples were merged by the cell ranger aggr function. The raw_feature_bc_matrix was loaded, and

the "Seurat" R package (v3.2.2) was further used for downstream analysis.[3] Cells were progressively further quality controlled based on three metrics, including total UMI counts, the number of genes detected, and the percentage of mitochondrial genes counted per cell. Specifically, cells with fewer than 400 genes detected were filtered out, and cells with a high detection rate (10%) of mitochondrial gene expression. Cells with more than 4000 genes detected were also filtered out to eliminate potential duality in our data.

Furthermore, genes detected in less than 10 cells were filtered out before further analysis. After quality control, data were normalized and scaled by the "SCTransform v2" function and percent of the ribosome and regressed out. We removed the batch effect across different individuals by identifying anchors between individuals and passing these anchors to the "IntegrateData" function. For visualization, the dimensionality was further reduced using Uniform Manifold Approximation and Projection (UMAP). We used an unsupervised graph-based clustering algorithm to cluster single cells by their expression profiles, Louvain. Single-cell RNA transcriptome data are available in the gene expression omnibus database under accession number GSE208565.

2.8 | Identification of signature genes and cell annotation

The marker genes for each cluster were obtained by the FindAllMarkers function in the Seurat package. Wilcox. test' algorithm was used to calculate statistical significance. Genes that met these criteria were considered as signature genes: (1) adjusted $p < 0.01$ after Bonferroni correction using all features in the data set; (2) log fold-change of the average expression > 0.25; (3) pct.1 > 0.25 (pct.1: the percentage of cells where the feature is detected in the first group); Functional enrichment was performed on these genes to get cell type enriched pathways. The main cell types were defined using the SingleR package.[4] Then we checked manually to ensure reported cell-type-specific expressed markers which were specificity on the corresponding clusters by the criteria: pct.1 > 0.6 and pct.2 < 0.4.

2.9 | Differential expression between groups

For scRNA-seq, differentially expressed genes (DEGs) were analyzed by the FindAllMarkers function in the Seurat package.[3] "MAST" algorithm was used to calculate statistical significance. Genes that met these criteria were considered DEGs: absolute log fold-change of the average expression ≥ 1.2 and pct > 0.2 (the percentage of cells where the feature is detected in either group); Functional enrichment was performed on these DEGs.

2.10 | Functional enrichment analysis

We used the Kyoto Encyclopedia of Genes and Genomes (KEGG) database and Gene Ontology (GO) category database for functional

annotation of DEGs. We performed enrichment analysis of GO categories on the R clusterProfiler (v3.14.3) package and enrichment analysis of pathways upon hypergeometric distribution by R "phyper" function. Those GO categories with a false discovery rate < 0.05 were significantly enriched. While pathways with a $p < 0.05$ were regarded as enriched. Only those GO categories or pathways containing ≥5 DEGs were kept for further analysis.

2.11 | PMN-MDSCs score

Genes associated with PMN-MDSCs and non-MDSCs were obtained from GSE148467. The difference multiplicity of genes in PMN-MDSCs versus non-MDSCs was then calculated. Genes that met these criteria were considered specifically highly expressed genes in PMN-MDSCs: $p < 0.001$, $\log_2 FC > 4$ and fragments per kilobase of exon model per million mapped fragments > 10. Then AUCell were used to quantify the corresponding gene set activity score. The score was plotted as violin.

2.12 | Cell proliferation score

GO term named "cell proliferation" gene signatures were collected from GO database. AUCell was used to quantify the related gene set activity score in AT2 cells between PBS and vaccine group. The score was plotted as violin.

2.13 | Damage-associated transient progenitors (DATPs) score

AUCell was used to quantify the DATPs marker genes (keratin 8 [*KRT8*], claudin 4 [*CLDN4*], cyclin dependent kinase inhibitor 1A [*CDKN1A*], and TNFAIP3 interacting protein 3 [*TNIP3*]) activity score in alveolar epithelial cells between PBS and vaccine group. The score was plotted as violin.

2.14 | Cell−ell communication

To uncover the communication interactions between cells and reveal the mechanism of the communicating molecules at a single-cell resolution, the R package "CellChat" (version 1.1.3) was applied.[5] "CellChatDB.human" database was used, and human genes were converted into the homologous gene from rhesus macaque. Two types of interactions were included: secreted signaling and extracellular matrix-receptor. CellChat was performed on each interaction separately. Using the "aggregateNet" function in CellChat, the aggregated cell−cell communication network was calculated and the signaling from each cell group was visualized. Outgoing or

incoming signals of certain cell types were recognized using the function "netAnalysis_signallingRole_heatmap."

2.15 | Pseudotime trajectory analysis

Pseudotime analysis was performed specially on endothelial cell lineage using R package Monocle 3. The unique expression matrix and cell identity defined by the Seurat package were used as input material for further analysis. And their pseudo-temporal trajectories were determined following integrating and reducing the dimensions with default parameters.

2.16 | BALF bulk RNA-seq data analysis

BALF was collected from rhesus macaques at Day 7 postinfection and then bulk RNA sequencing was performed. For the bulk-seq data, the differential expression genes were determined by edgeR and DESeq2 R package. mRNAs with a cutoff of fold change ≥ 1.5 and $p < 0.05$ were considered differentially expressed. RNA-seq data are available in the GEO database under accession number GSE209615.

2.17 | Statistical analysis

Statistical analysis was performed using the unpaired Student's *t*-test with data from two groups, while data from more than two groups were analyzed using an ANOVA followed by Tukey's method for multiple comparisons. Significance was accepted when $p < 0.05$. *$p < 0.05$, **$p < 0.01$, ***$p < 0.001$.

3 | RESULTS

3.1 | SW0123 confers effective protection in the lungs of rhesus macaques upon SARS-CoV-2 infection

We have shown that SW0123 demonstrated strong immunogenicity and protective capacity in animal models.[2] Of particular note, upon SARS-CoV-2 challenge, rhesus macaques receiving three doses of SW0123 displayed intact pulmonary alveoli structure with only mild focal tissue damages and decreased immune response cell infiltration as compared with unvaccinated control group (Figure 1A). In addition, a significant thrombus level was observed in unvaccinated rhesus macaques (Figure 1A), consistent with clinical observations in COVID-19 patients.[6] Then lung pathology scoring further revealed a dramatically decreased level of pathological damage in SW0123-vaccinated rhesus macaques (Figure 1A). The protein levels of IL-15 and monocyte chemoattractant protein-1(MCP-1) in BALF from vaccinated group were lower than that in unvaccinated group (Figure 1B). To further explore the level of

inflammation in local lung tissue, bulk RNA sequencing was performed on BALF. DEG analysis showed that the expression of proinflammatory factors (interleukin 2 receptor subunit gamma [*IL2RG*], C-C motif chemokine ligand 5 [*CCL5*], TNF receptor superfamily member 1A [*TNFRSF1*], TNF alpha induced protein 2 [*TNFAIP2*], and interleukin 2 receptor subunit beta [*IL2RB*]) was decreased, while the expression of interleukin 1 receptor type 2 (*IL1R2*), interleukin 1 receptor antagonist (*IL1RN*), and inflammation and lipid regulator with ubiquitin-associated domain-like and NBR1-like domains (*ILRUN*) was increased in the vaccine group (Figure 1C, Supporting Information: Table S1). IL-1 is one of the key cytokines that contribute to the formation of cytokine storms during SARS-CoV-2 infection, which can be counteracted by IL1R2 or IL1RN. Previous studies found that ILRUN could downregulate angiotensin converting enzyme 2 (ACE2) expression and block the infection of human cells by SARS-CoV-2.[7] These results indicate that SW0123 vaccination alleviates lung damage and inflammation caused by SARS-CoV-2 infection.

3.2 | SW0123 vaccination alters the single-cell landscape of the lungs upon SARS-CoV-2 infection

To investigate the effects of SARS-CoV-2 infection on the lung and explore the underlying mechanisms associated with vaccine-induced protection, we performed scRNA-seq on the lung tissues collected from rhesus macaques at Day 7 postinfection. Clustering analysis showed 23 major cell populations in the lung of rhesus macaque (Figure 2A), which are natural killer (NK) cells (*NKG7*, *GZMB*, and *KLRC1*), CD8+ T cells (*CD3D*, *CD3E*, *CD8A*, and *GZMK*), CD4+ T cells (*CD3D*, *CD3E*, *CD4*, and *IL7R*), B cells (*MS4A1* and *CD79B*), macrophages (*CSTB*, *CD68*, and *MRC1*), monocytes (*CD14* and *FCN1*), neutrophils (*S100A8*, *S100A9*, and *CSF3R*), endothelial cells (*PECAM1* and *VWF*), AT2 cells (*SFTPB*), lymphatic endothelial cells (*CCL21*, *LYVE1*, and *FROX1*), AT1 cells (*AGER*, *AQP4*, and *HOPX*), myofibroblasts (*TAGLN*, *COL6A2*, *ACTA2*, and *FGF7*), and others (Supporting Information: Figure S1A). Compared with the PBS group,
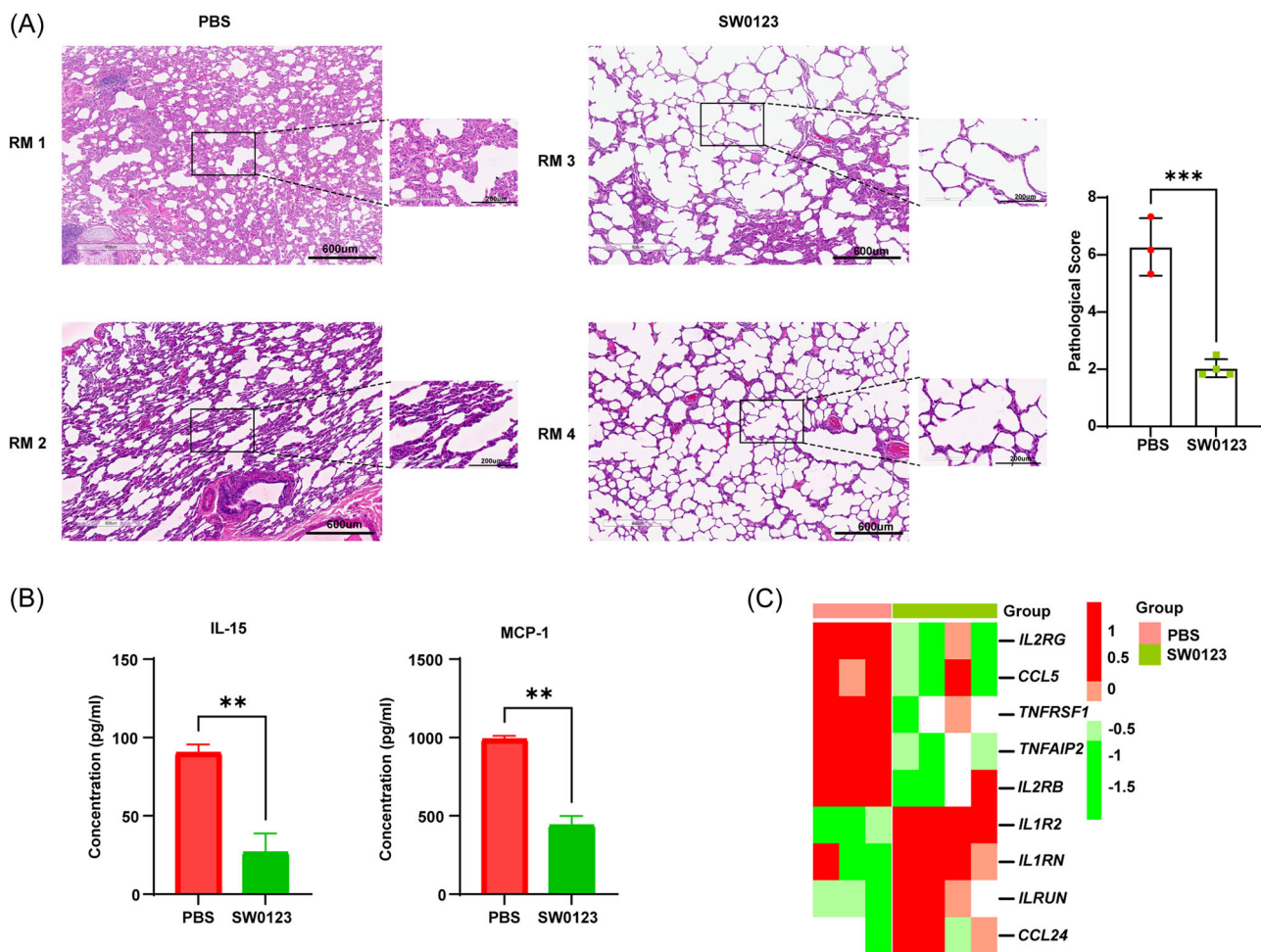

FIGURE 1 SW0123 confers effective protection in the lungs of rhesus macaques upon SARS-CoV-2 infection. (A) Representative images and pathological score quantification of HE staining of lung tissues from rhesus macaques with SW0123 vaccination or PBS administration 7 days post-SARS-CoV-2 infection. (B) ELISA of IL-15 and MCP-1 in BALF of rhesus macaques with SW0123 vaccination or PBS administration 7 days post-SARS-CoV-2 infection. (C) The heatmap showed the expression levels of inflammation-associated genes in BALF of rhesus macaques with SW0123 vaccination or PBS administration 7 days post-SARS-CoV-2 challenge. BALF, Bronchoalveolar lavage fluid; HE, hematoxylin and eosin; MCP-1, monocyte chemoattractant protein-1; SARS-CoV-2, severe acute respiratory syndrome coronavirus-2.

vaccinated animals demonstrated a higher level of AT1 cells, endothelial cells, and a lower level of CD8+ T cells and myeloid dendritic cells in the lungs (Figures 2B,C). Other major cell subsets showed no significant changes between the two groups.
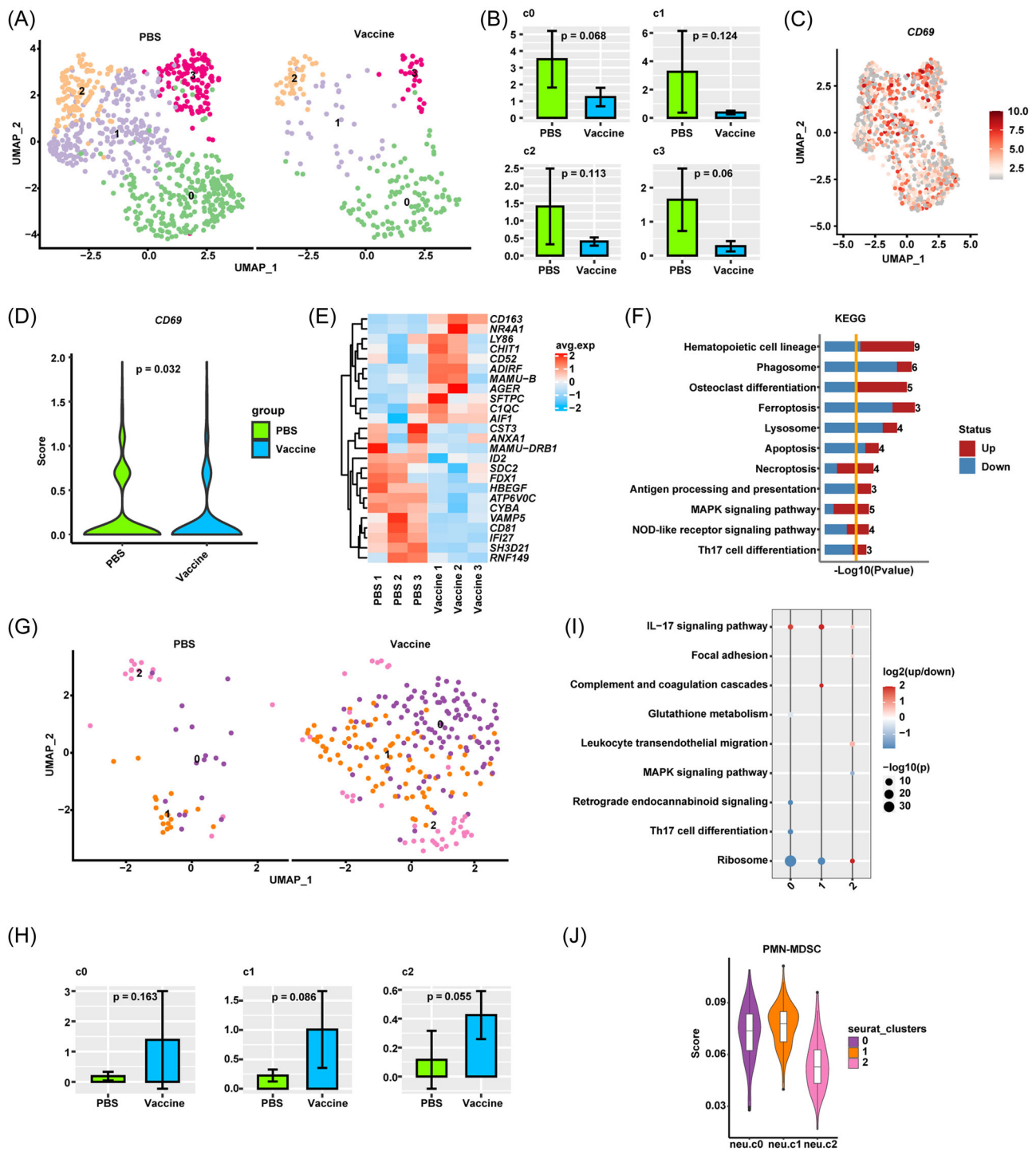
3.3 | SW0123 vaccination alters the distribution of macrophages and neutrophils in the lungs upon SARS-CoV-2 infection

SARS-CoV-2-induced inflammation was largely attributed to dysregulated macrophage activation and critically associated with COVID-19 severity.[8] The heterogeneity of the lungs' macrophages

was depicted by UMAP, and four major macrophage subsets were identified (Figure 3A, Suporting Information: Figure S1B). All the four subsets ratio showed a decreased trend in the vaccinated rhesus macaques compared with that in PBS group (Figure 3B). Expression of CD69, a typical marker for macrophage activation, was significantly lower in the lung macrophages from the vaccinated rhesus macaques when analyzed as a whole[9] (Figure 3C,D). The expression of annexin A1 (*ANXA1*) and cystatin C (*CST3*), which mediate anti-inflammatory responses, was markedly decreased in the vaccinated rhesus macaques upon the SARS-CoV-2 challenge[10,11] (Figure 3E, Suporting Information: Table S2). Moreover, KEGG analysis showed that DEGs of macrophages enriched in the phagosome were notably downregulated in the vaccinated rhesus macaques (Figure 3F,
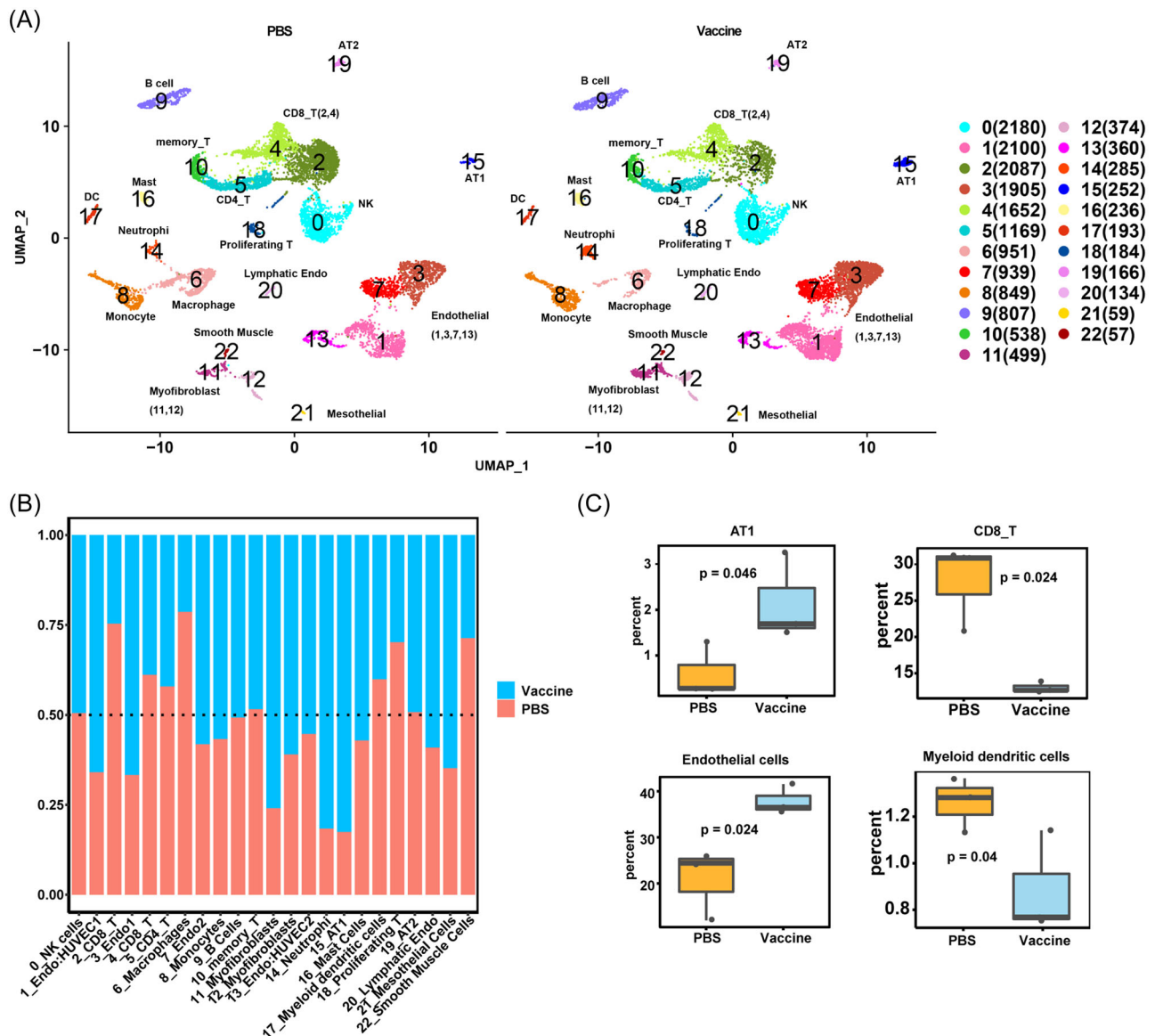
FIGURE 2 SW0123 vaccination alters the single-cell landscape of the lungs upon SARS-CoV-2 infection. (A) Twenty-three distinct cell clusters identified in lung tissues from rhesus macaques with SW0123 vaccination or PBS administration were visualized by UMAP plotting, with each cell color-coded for its associated clusters. (B, C) The proportions of the major lung cell types among rhesus macaques with SW0123 vaccination or PBS administration upon SAR-CoV-2 infection. SAR-CoV-2, severe acute respiratory syndrome coronavirus-2; UMAP, Uniform Manifold Approximation and Projection.

FIGURE 3 SW0123 vaccination alters the distribution of macrophages and neutrophils in the lungs upon SARS-CoV-2 infection. (A) UMAP plot of cell clusters from different phenotypes of macrophages identified in lung tissues from rhesus macaques with SW0123 vaccination or PBS administration. The color of cells reflected the individual origin. (B) Quantifying proportion from four macrophage phenotypes among rhesus macaques with SW0123 vaccination or PBS administration. (C) The UMAP plot showed the expression of *CD69* in macrophages. (D) The Violin plot showed *CD69* expression level in the lung macrophages with SW0123 vaccination or PBS treatment post-SARS-CoV-2 challenge in rhesus macaques. (E) Heatmap of DEGs among macrophages in rhesus macaques with SW0123 vaccination or PBS administration. (F) KEGG pathway analysis showed the participation of DEGs in indicated signaling pathways among lung macrophages from rhesus macaques with SW0123 vaccination or PBS administration. (G) UMAP plot of cell clusters from different phenotypes of neutrophils identified in lung tissues from rhesus macaques with SW0123 vaccination or PBS administration. The color of cells reflected the individual origin. (H) Quantifying proportion of three neutrophil phenotypes among rhesus macaques with SW0123 vaccination or PBS administration. (I) KEGG pathway analysis showed the participation of DEGs in indicated signaling pathways among lung neutrophils from rhesus macaques with SW0123 vaccination or PBS administration. (J) The Violin plot showed the assessment of PMN-MDSC characteristics in the three phenotypes of neutrophils. DEGs, differentially expressed genes; KEGG, Kyoto Encyclopedia of Genes and Genomes; SARS-CoV-2, SAR-CoV-2, severe acute respiratory syndrome coronavirus-2; UMAP, Uniform Manifold Approximation and Projection.

Suporting Information: Table S2). These data indicate that SW0123 vaccination significantly inhibits the infiltration and activation of the lung macrophage population.

Previous studies have confirmed that the formation of neutrophil extracellular traps (NETs) was associated with COVID-19 severity and was involved in the microthrombi formation and platelet deposition in COVID-19 patients.[12] The UMAP plot showed that neutrophils in the lung of rhesus macaques were classified into three subsets (cluster 0, cluster 1, and cluster 2) (Figure 3G, Supporting Information: Figure S1C). Cell frequencies of clusters 0, 1, and 2 have an increased tendency in the vaccinated rhesus macaques (Figure 3H). Notably, KEGG enrichment analysis showed that DEGs exhibited no significant changes in signaling pathways associated with inflammatory responses in the vaccinated rhesus macaques (Figure 3I, Supporting Information: Table S2). We speculated that the neutrophils presented in the lungs following infection were immune-suppressive cells that might act as an immune-balancing role in ameliorating excessive inflammation. The further analysis supported that these neutrophils showed the characteristics of PMN-MDSCs (Figure 3J). Altogether, these data demonstrate that SW0123 vaccination alters the distribution of innate immune cells in the lungs, which may play a protective role in controlling SARS-CoV-2-induced inflammation.

3.4 | SW0123 vaccination attenuates the damage to lung epithelial cells caused by SARS-CoV-2

AT1 and AT2 are two major cell targets of SARS-CoV-2. AT1 cells perform critical gas exchange functions in the lung. These cells occupy 95%–97% of the total surface area of the peripheral lung. As terminally differentiated cells, AT1 cells cannot self-renew. In contrast, AT2 cells, despite occupying a very small area, are the primary epithelial progenitor cells, capable of long-term self-renewal and pluripotent differentiation, giving rise to AT1 cells.[13] GO analysis showed that DEGs enriched in cell death of AT1 cells from the vaccinated rhesus macaques were downregulated (Figure 4A, Supporting Information: Table S3). In addition, the frequency of AT1 cells was dramatically increased in SW0123 vaccinated-rhesus macaques (Figure 2C). It was reported that the limited thioredoxin-1 (TXN) expression augmented oxidative DNA damage and ribosomal protein L6 (RPL6) expression level represented the extent of the DNA damage response.[14,15] We found that TXN showed a significantly increased expression and RPL6 showed a significantly decreased expression in the vaccine group (Figure 4B, Supporting Information: Table S3), indicating that SW0123 vaccination mitigated DNA damage in AT1 cells induced by SARS-CoV-2 infection. Since AT2 cells can proliferate and differentiate into AT1 cells to compensate for the loss of AT1 cells, the proliferative ability of AT2 cells is critical for tissue repair after lung injury.[16] Cell proliferation-related genes were further evaluated, and many of them (SDC4, hedgehog interacting protein [HHIP], cathepsin H [CTSH]) showed an increased

expression in AT2 cells in the vaccine group (Figure 4C, Supporting Information: Table S3), the proliferative ability of AT2 cells was significantly enhanced after vaccination as well (Figure 4D). Inflammatory signals were reported to induce AT2 cell-derived DATPs that mediated alveolar regeneration, which caused AT2 cells' inability to transit to AT1 cells.[17] Expression of the DATP marker genes (KRT8, CLDN4, CDKN1A, and TNIP3) in alveolar epithelial cells from the vaccinated rhesus macaques was significantly lower than that in PBS group (Figure 4E). Also, GO analysis showed that DEGs enriched in cell death of AT2 cells from the vaccinated rhesus macaques were downregulated (Figure 4F, Supporting Information: Table S3). In summary, SW0123 vaccination alleviates the damage of lung epithelial cells caused by SARS-CoV-2 infection.

3.5 | SW0123 vaccination maintains endothelial barrier function post-SARS-CoV-2 infection

Endothelium participates in the formation of thrombosis and fibrinolysis caused by SARS-CoV-2 infection.[18] Maintaining the homeostasis of the endothelial compartment has been proposed to be helpful in COVID-19 treatment.[18] Therefore, we profiled the signature of endothelial cells in the lungs from rhesus macaques. The UAMP plot showed that endothelial cells were classified into 9 populations (Figure 5A, Supporting Information: Figure S2A), many of which showed a dramatic increase in cell frequency in the vaccinated rhesus macaques (Supporting Information: Figure S2B). Then monocle was used to reconstruct a trajectory which mainly contained 3 branches (denoted B1, B2, and B3) (Supporting Information: Figure S2C). B1 was populated by cells from cluster 0 and cluster 2. B3 was populated by cells from cluster 1, 3, and 6, which had a specific expression of some proteins released in response to injury (such as regulator of G-protein signaling 5 [RGS5] and leukemia inhibitory factor receptor subunit alpha [LIFR]). Based on the above findings, we speculate that cluster 0 and cluster 2 belong to naive endothelial cells while cluster 1, cluster 3, and cluster 6 belong to activated endothelial cells. Cluster 4 (mainly from B2, which located between two main branches) was identified as "transitional state" endothelial cells. Under physiological conditions, the endothelial portal selectively regulates endothelial permeability and promotes vascular integrity. An intact endothelial barrier depends on various mechanisms, including vascular endothelial-cadherin (VE-cadherin) and adherens junction.[19] The expression of CDH5 (cadherin 5, encoding VE-cadherin) from the vaccinated rhesus macaques was much higher than that in PBS group (Figure 5B). In addition, bulk transcriptomic sequencing of BALF from rhesus macaques showed that DEGs enriched in adherents and tight junctions were greatly upregulated in the vaccine group after SARS-CoV-2 infection (Figure 5C, Supporting Information: Table S1). P-selectin (SELP) and vascular cell adhesion molecule 1 (VCAM1), two specific biomarkers widely used to assess endothelial cell activation and dysfunction. We found SELP were much lower and VCAM1 showed a lower trend in
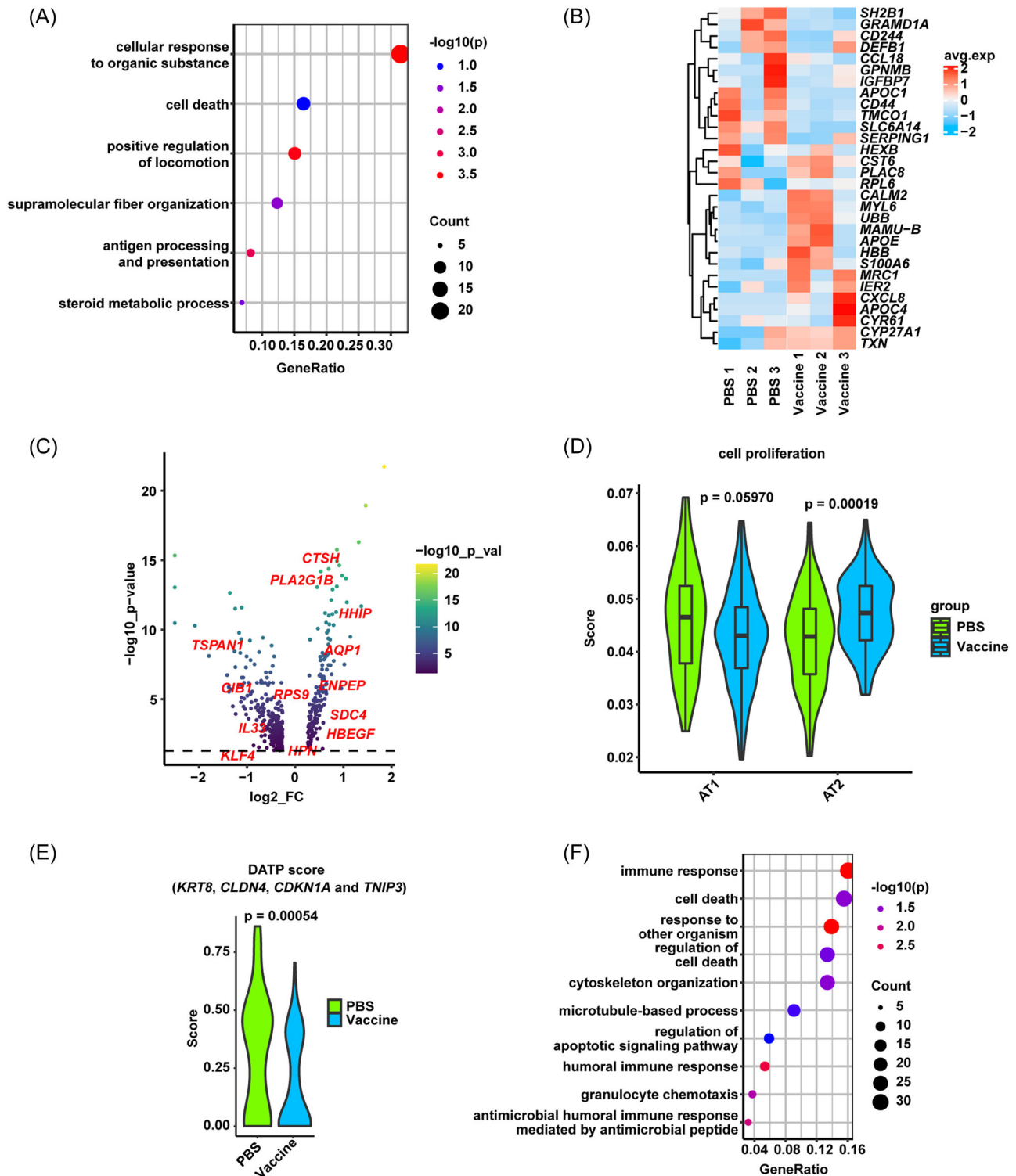
FIGURE 4 SW0123 vaccination attenuates the damage to lung epithelial cells caused by SARS-CoV-2. (A) GO enrichment analysis of DEGs in AT1 cells between SW0123 vaccination and PBS administration in rhesus macaques. (B) Heatmap of DEGs in AT1 cells between SW0123 vaccination and PBS administration in rhesus macaques. (C) Volcano plots of cells proliferation-associated DEGs in AT2 cells with SW0123 vaccination upon SARS-CoV-2 infection. (D) Violin plot showed the scoring of cell proliferation capacity in AT1 and AT2 cells in lungs from rhesus macaques with SW0123 vaccination or PBS administration. (E) Violin plots showing the expression scores of DATP-associated genes (*KRT8*, *CLDN4*, *CDKN1A*, and *TNIP3*) in AT2 cells between SW0123 vaccination and PBS administration in rhesus macaques. (F) GO enrichment analysis of DEGs in AT2 cells between SW0123 vaccination and PBS administration in rhesus macaques. AT1, alveolar type 1; DEGs, differentially expressed genes; GO, Gene Ontology; SARS-CoV-2, severe acute respiratory syndrome coronavirus-2.
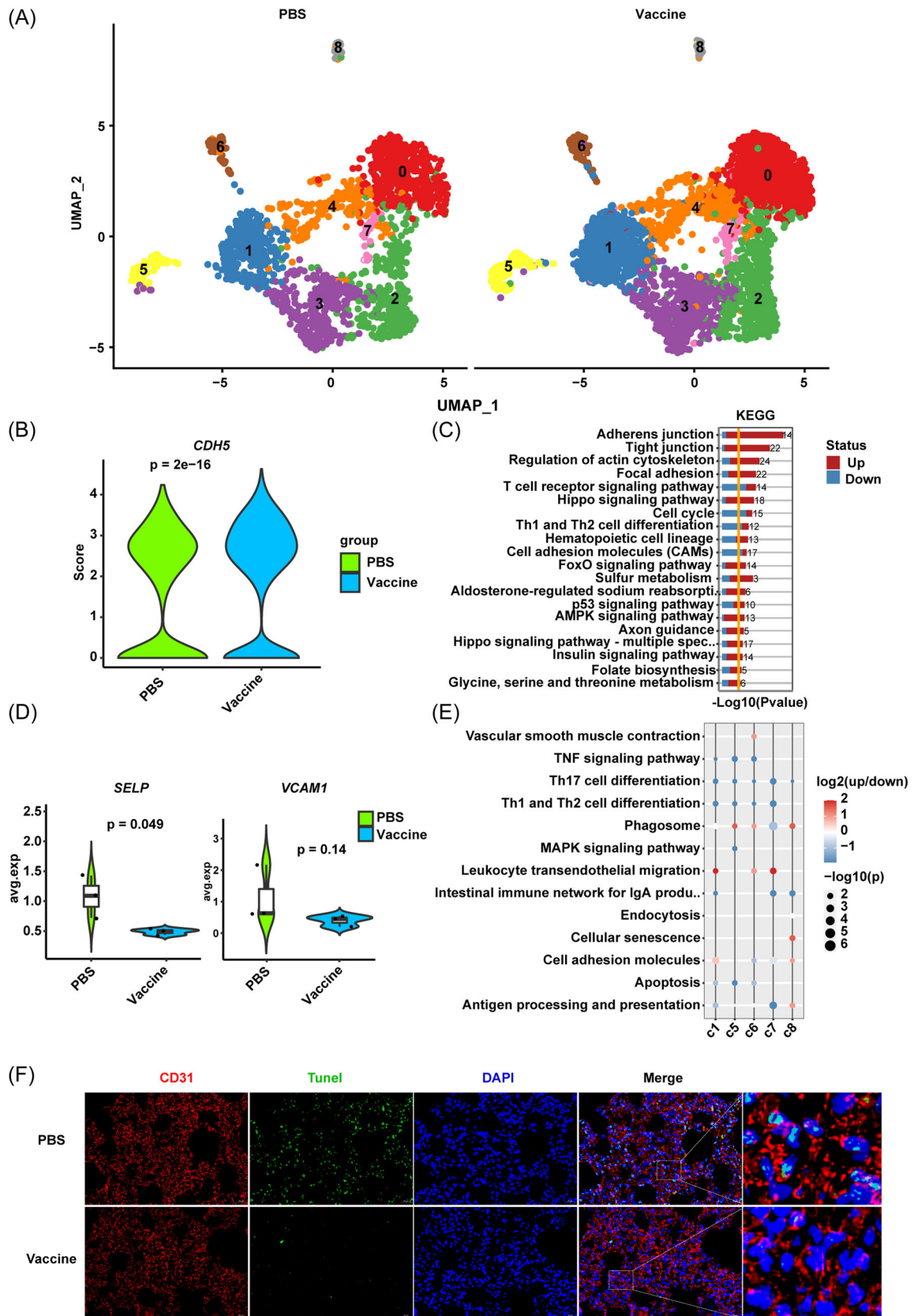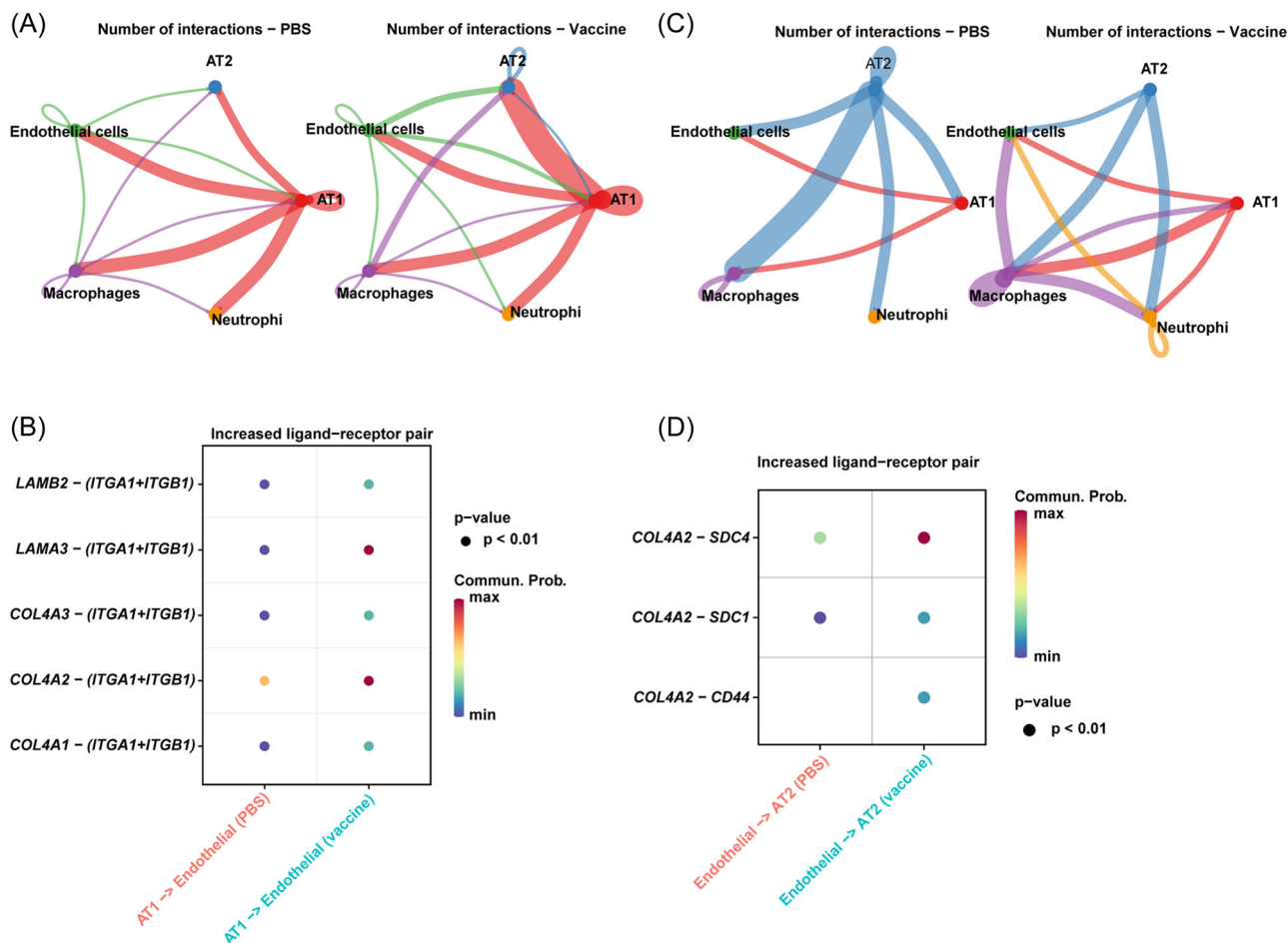
(A)

(B)

(C)

(D)

(E)

(F)

FIGURE 5 (See caption on next page)

FIGURE 6 Cell–cell communication is altered by the SW0123 vaccination. (A) Map of cell–cell interaction (CCI) network uncovering extracellular matrix-receptor-dependent cell–cell communication among different types of cells in the vaccine group and control group. (B) Analysis of the ligand-receptor pair interaction between AT1 and endothelial cells in the vaccine and control groups. (C) Map of CCI network uncovering chemical signal-dependent cell–cell communications between different types of cells in the vaccine group and control group. (D) Analysis of the ligand-receptor pair interaction between endothelial cells and AT2 cells in the vaccine and control groups. AT1, alveolar type 1.

expression of endothelial cells from the lungs in the vaccine group[20] (Figure 5D). Endothelial cells are located at the interface between blood and tissue and usually resist prolonged contact with the blood leukocytes that bathe the endothelial surface.[21] Proinflammatory cytokines could disrupt the homeostasis of the endothelium compartment to cause thrombosis and local tissue damage.

Interestingly, KEGG analysis showed a significant decrease in the expression of genes relevant to inflammatory signaling pathways in all endothelial cell subsets after vaccination (Figure 5E, Supporting Information: Table S4). Consistent with this, cell apoptosis of endothelial cells in the vaccine group was much suppressed (Figure 5F). To sum up, these data indicate that SW0123 vaccination

FIGURE 5 SW0123 vaccination maintains endothelial barrier function post-SARS-CoV-2 infection. (A) UMAP plots displaying endothelial cell clusters in rhesus macaques with SW0123 vaccination or PBS administration infected by SARS-CoV-2. (B) Violin plot showing scoring of *CDH5* gene in endothelial cells between SW0123 vaccination and PBS administration in rhesus macaques. (C) KEGG pathway analysis of the participation of DEGs in indicated signaling pathways from BALF in rhesus macaques with SW0123 vaccination or PBS administration. (D) Violin plot showing scoring of *SELP* and *VCAM1* genes in endothelial cells between SW0123 vaccination and PBS administration in rhesus macaques. (E) KEGG pathway analysis of the participation of DEGs in inflammation-related signaling pathways from endothelial cells between SW0123 vaccination and PBS treatment in rhesus macaques. (F) Representative images of immunofluorescence staining of CD31 and TUNEL in endothelial cells from rhesus macaques with SW0123 vaccination or PBS administration upon SARS-CoV-2 challenge. DEGs, differentially expressed genes; KEGG, Kyoto Encyclopedia of Genes and Genomes; SARS-CoV-2, severe acute respiratory syndrome coronavirus-2; UMAP, Uniform Manifold Approximation and Projection.

inhibits the apoptosis of endothelial cells and maintains endothelial barrier function.

3.6 | Cell-cell communication is altered by the SW0123 vaccination

Cell−cell communication in the lung compartment of COVID-19 patients is significantly altered during disease progression. We further explored the interactions between major cell subsets with change as aforementioned. The cell-matrix interaction showed an increased tendency between AT1 and AT2 cells (Figure 6A). The ligand-receptor pair interaction revealed that *LAMB2*, *LAMA3*, *COL4A3*, *COL4A2*, or *COL4A1* expressed by AT1 cells could interact with *ITGA1* and *ITGB1* on endothelial cells (Figure 6B). Previous studies have shown that the *ITGA1* gene encodes the alpha 1 subunit of integrin receptors and could regulate cell migration.[22] ITGB1 plays an important role in protecting arterial endothelial cell polarity and lumen formation of nascent endothelium.[23] While the signaling of *ITGA1* and *ITGB1* interacted with other ligands was dramatically enhanced in the vaccine group than that in PBS control group, which suggested that SW0123 vaccination protected against the loss of endothelial cells likely through the enhanced ligand-receptor interactions (Figure 6B). In addition, chemical signal-mediated interactions between AT1 and AT2 cells, macrophages and AT2 cells were markedly decreased, while interaction was increased between AT1 and macrophages (Figure 6C). There was evidence of autologous interaction between endothelial cells via soluble factors. Soluble ligand-receptor pair interaction revealed that *COL4A2* expressed by endothelial cells interacted with *SDC4*, *SDC1*, or *CD44* on AT2 cells (Figure 6D). Since *SDC4* and *SDC1* regulate cell proliferation and migration, autologous endothelial cell interaction may account for the increased angiogenic and vascular barrier capacity of endothelial cells after vaccination. Altogether, these data indicate the lung damage after SARS-CoV-2 infection is alleviated, at least partly, through cell−cell communications after SW0123 vaccination.

4 | DISCUSSION

One main characteristic of COVID-19 patients is hypoxemia, which can develop into acute respiratory distress in severe cases.[24] Severe COVID-19 patients are normally presented with hyper-inflammatory status with excessive cytokine production, both systemically and locally in the lung, which is correlated with disease severity.[25,26] Innate immune cells such as macrophages and neutrophils are sentinels responding quickly to infection and are critically involved in generating inflammation that can help clear the infection. However, such a response may be dysregulated during infection and leads to a cytokine storm with excessive release of proinflammatory cytokines.[25] Macrophages are one of the major causes of dysregulated inflammatory responses in COVID-19. For example, monocyte-derived macrophages were highly activated in the lung of COVID-19 patients. Tumor-associated macrophage receptor anexelekto could play a key role in anti-inflammatory regulation during tissue repair and was significantly reduced in lung-resident alveolar macrophages post-SARS-CoV-2 infection.[27] Neutrophils could produce cytotoxic factors and chemokines (C-X-C motif chemokine receptor 2 [CXCR2] and IL-8), exacerbating lung inflammation in severe COVID-19 patients.[28] The neutrophil/lymphocyte ratio has proved to be an important parameter predicting disease severity and outcome in COVID-19 patients.[29] SARS-CoV-2–activated neutrophils could induce cell death of lung epithelial cells through the release of NETs.[30] Our study observed a lower proportion of lung macrophages with the decreased activation in SW0123-vaccinated rhesus macaques upon infection. In vaccinated animals, neutrophils recruited to the lung showed immune-suppressive PMN-MDSC characteristics. Additionally, we found that the levels of proinflammatory cytokines were significantly decreased in the BALF of vaccinated rhesus macaques. Of course, the immune cells involved after COVID-19 infection are not only macrophages and neutrophils. As our study was based on the analysis of single-cell data from the lung, the exploration of adaptive immune responses mediated by B cells and T cells was difficult to perform. The COVID-19 mRNA vaccine primarily focuses on triggering B cells to promote the induction of neutralizing antibodies, but there are also good reasons to believe that CD4+ T cell and CD8+ T cell-mediated responses contribute to the protection against SARS-CoV-2. In COVID-19 patients, coordinated adaptive immunity with CD4+ T cells, CD8+ T cells and antibody responses was associated with milder disease, while uncoordinated responses often failed to control disease.[31] Some studies showed no significant decrease in T-cell-triggered specific responses several months after vaccination.[32] Hence some researchers have developed COVID-19 vaccines specifically to induce T-cell immunity and thus help people with antibody deficiency.[33]

SARS-CoV-2 was reported to infect AT1, AT2, and endothelial cells, leading to lung damage.[34] ACE2 expression in AT2 is significantly increased with the hypoxic condition, promoting viral binding to AT2 cells and prolonging the duration of respiratory failure.[35] Moreover, granulocyte-macrophage colony-stimulating factor expression, which is necessary for maintaining the normal function of macrophages, was markedly reduced in alveolar epithelial cells.[36] In vitro studies have shown that epithelial cells can mediate inflammatory responses and produce cytokines/chemokines.[37] Under physiological conditions, endothelial cells have important functions such as regulating vascular permeability and integrity, anticoagulation, and antithrombosis. Many apoptotic endothelial cells were found in SARS-CoV-2-infected lungs, which led to endothelial cell dysfunction and further aggravated lung injury.[38]

Furthermore, activated endothelial cells can produce IL-1α and IL-1β precursors, contributing to the excessive production of cytokines.[18] Cell death promotion genes were downregulated in alveolar epithelial cells and endothelial cells in SW0123 vaccinated-rhesus macaques. These findings indicate that SW0123 vaccination prevents cell death of alveolar and endothelial cells following

infection, thereby reducing tissue damage. The detailed mechanism underlying the reduced cell death in SW0123 vaccinated-animals needs to be further investigated.

It has been shown that epithelium-immune cell interactions increase the infectivity of epithelial cells. Immune cell-epithelial cell interactions were more frequent in patients with severe COVID-19 compared to those with moderate COVID-19, and the interactions between different immune cell subsets were also promoted, especially macrophage-cytotoxic T cell interactions.[39] In COVID-19 patients, the degree of epithelial and immune cell interactions was higher in men, which might be a reason for the higher incidence of SARS-CoV-2 infection and the likelihood of severe COVID-19 outcomes in male individuals.[40] However, the interaction between alveolar epithelial cells and endothelial cells after SARS-CoV-2 infection has not been much studied. Our study found the reduced interaction between macrophages and AT2 cells and enhanced interaction between alveolar epithelial cells and endothelial cells through ligand-receptor after SW0123 vaccination. Although the interactions of ligand-receptor pairs between different cell types are affected after SW0123 vaccination, the detailed effect mediated by each pair interaction remains to be further investigated.

In addition, the most important question about mRNA vaccines is undoubtedly whether they are safe for human. The side effects of mRNA vaccination, such as myocarditis, lymphocytic colitis and fasciitis, are becoming apparent.[41–43] On the one hand, mRNA vaccines need the innate immune system to enhance their ability to induce and tailor antigen-specific responses. On the other hand, a systemic and persistent inflammatory response can have adverse consequences for the body. More efficient mRNA delivery systems and the modification and optimization of nucleosides to avoid triggering a sustained innate immune response may be an urgent challenge for future mRNA vaccines. Perhaps more ways can be developed to further reduce the innate immune reactivity of mRNA vaccines without compromising vaccine efficacy?

Altogether, our study unravels the protective characteristics independent of the adaptive immunity of a novel mRNA vaccine, SW0123, which helps people better trigger the generation of host protective responses to SARS-CoV-2 infection.

AUTHOR CONTRIBUTIONS

Xingguang Liu, Zhenzhen Zhan, and Ang Lin designed the research and revised the manuscript. Yong Tan, Shuaiyao Lu, Bo Wang, Xuewen Duan, and Yunkai Zhang performed experiments and analyzed the data. Yong Tan wrote the original draft of the manuscript. Xiaozhong Peng offered the constructive proposals for experimental design. Hangwen Li provided the mRNA vaccine SW0123. All authors have critically read and approved the final version of manuscript.

CONFLICT OF INTEREST

Stemirna Therapeutics filed patents on patent application entitled "A prophylactic or therapeutical 2019-nCoV mRNA vaccine". The ramaining authors declare no conflict of interest.

DATA AVAILABILITY STATEMENT

The data that support the findings of this study are available from the corresponding author, Xingguang Liu, upon reasonable request.

ETHICS STATEMENT

There is no experimental work with humans included in this article. All animal studies were performed in accordance with the Guide for the Care and Use of Laboratory Animals and approved by the Institutional Animal Care and Use Committee.

ORCID

Zhenzhen Zhan https://orcid.org/0000-0002-4943-1659
Xingguang Liu http://orcid.org/0000-0002-1928-8847

REFERENCES

1. Zhang B, Zhou X, Qiu Y, et al. Clinical characteristics of 82 cases of death from COVID-19. PLoS One. 2020;15(7):e0235458.
2. Yang R, Deng Y, Huang B, et al. A core-shell structured COVID-19 mRNA vaccine with favorable biodistribution pattern and promising immunity. Signal Transduct Target Ther. 2021;6(1):213.
3. Stuart T, Butler A, Hoffman P, et al. Comprehensive integration of single-cell data. Cell. 2019;177(7):1888-1902.
4. Aran D, Looney AP, Liu L, et al. Reference-based analysis of lung single-cell sequencing reveals a transitional profibrotic macrophage. Nat Immunol. 2019;20(2):163-172.
5. Jin S, Guerrero-Juarez CF, Zhang L, et al. Inference and analysis of cell−cell communication using CellChat. Nat Commun. 2021;12(1): 1088.
6. Gómez-Mesa JE, Galindo-Coral S, Montes MC, Muñoz Martin AJ. Thrombosis and coagulopathy in COVID-19. Curr Probl Cardiol. 2021;46(3):100742.
7. Tribolet L, Alexander MR, Brice AM, et al. ILRUN downregulates ACE2 expression and blocks infection of human cells by SARS-CoV-2. J Virol. 2021;95(15):e0032721.
8. Hoang TN, Pino M, Boddapati AK, et al. Baricitinib treatment resolves lower-airway macrophage inflammation and neutrophil recruitment in SARS-CoV-2-infected rhesus macaques. Cell. 2021;184(2):460-475.
9. Hu Y, Wei X, Liao Z, et al. Transcriptome analysis provides insights into the markers of resting and LPS-Activated macrophages in grass carp (Ctenopharyngodon idella). Int J Mol Sci. 2018;19(11):3562.
10. Yang YH, Aeberli D, Dacumos A, Xue JR, Morand EF. Annexin-1 regulates macrophage IL-6 and TNF via glucocorticoid-induced leucine zipper. J Immunol. 2009;183(2):1435-1445.
11. Biasizzo M, Trstenjak-Prebanda M, Dolinar K, et al. Cystatin C deficiency increases LPS-Induced sepsis and NLRP3 inflammasome activation in mice. Cells. 2021;10(8):2071.
12. Middleton EA, He XY, Denorme F, et al. Neutrophil extracellular traps contribute to immunothrombosis in COVID-19 acute respiratory distress syndrome. Blood. 2020;136(10):1169-1179.

13. Williams MC. Alveolar type I cells: molecular phenotype and development. *Annu Rev Physiol*. 2003;65:669-695.

14. Kamal AM, El-Hefny NH, Hegab HM, El-Mesallamy HO. Expression of thioredoxin-1 (TXN) and its relation with oxidative DNA damage and treatment outcome in adult AML and ALL: a comparative study. *Hematology*. 2016;21(10):567-575.

15. Yang C, Zang W, Ji Y, Li T, Yang Y, Zheng X. Ribosomal protein L6 (RPL6) is recruited to DNA damage sites in a poly(ADP-ribose) polymerase-dependent manner and regulates the DNA damage response. *J Biol Chem*. 2019;294(8):2827-2838.

16. Barkauskas CE, Cronce MJ, Rackley CR, et al. Type 2 alveolar cells are stem cells in adult lung. *J Clin Invest*. 2013;123(7):3025-3036.

17. Choi J, Park JE, Tsagkogeorga G, et al. Inflammatory signals induce AT2 cell-derived damage-associated transient progenitors that mediate alveolar regeneration. *Cell Stem Cell*. 2020;27(3):366-382.

18. Libby P, Lüscher T. COVID-19 is, in the end, an endothelial disease. *Eur Heart J*. 2020;41(32):3038-3044.

19. Giannotta M, Trani M, Dejana E. VE-cadherin and endothelial adherens junctions: active guardians of vascular integrity. *Dev Cell*. 2013;26(5):441-454.

20. Liao JK. Linking endothelial dysfunction with endothelial cell activation. *J Clin Invest*. 2013;123(2):540-541.

21. Pober JS, Sessa WC. Evolving functions of endothelial cells in inflammation. *Nat Rev Immunol*. 2007;7(10):803-815.

22. Liu X, Tian H, Li H, et al. Derivate isocorydine (d-ICD) suppresses migration and invasion of hepatocellular carcinoma cell by down-regulating ITGA1 expression. *Int J Mol Sci*. 2017;18(3):514.

23. Zovein AC, Luque A, Turlo KA, et al. Beta1 integrin establishes endothelial cell polarity and arteriolar lumen formation via a Par3-dependent mechanism. *Dev Cell*. 2010;18(1):39-51.

24. Zhou F, Yu T, Du R, et al. Clinical course and risk factors for mortality of adult inpatients with COVID-19 in Wuhan, China: a retrospective cohort study. *Lancet*. 2020;395(10229):1054-1062.

25. Huang C, Wang Y, Li X, et al. Clinical features of patients infected with 2019 novel coronavirus in Wuhan, China. *Lancet*. 2020;395(10223):497-506.

26. Del Valle DM, Kim-Schulze S, Huang HH, et al. An inflammatory cytokine signature predicts COVID-19 severity and survival. *Nat Med*. 2020;26(10):1636-1643.

27. Melms JC, Biermann J, Huang H, et al. A molecular single-cell lung atlas of lethal COVID-19. *Nature*. 2021;595(7865):114-119.

28. Wang LL, Yang JW, Xu JF. Severe acute respiratory syndrome coronavirus 2 causes lung inflammation and injury. *Clin Microbiol Infect*. 2022;28(4):513-520.

29. Zhang B, Zhou X, Zhu C, et al. Immune phenotyping based on the Neutrophil-to-Lymphocyte ratio and IgG level predicts disease severity and outcome for patients with COVID-19. *Front Mol Biosci*. 2020;7:157.

30. Veras FP, Pontelli MC, Silva CM, et al. SARS-CoV-2-triggered neutrophil extracellular traps mediate COVID-19 pathology. *J Exp Med*. 2020;217(12):e20201129.

31. Rydyznski Moderbacher C, Ramirez SI, Dan JM, et al. Antigen-Specific adaptive immunity to SARS-CoV-2 in acute COVID-19 and associations with age and disease severity. *Cell*. 2020;183(4): 996-1012.

32. GeurtsvanKessel CH, Geers D, Schmitz KS, et al. Divergent SARS-CoV-2 omicron-reactive T and B cell responses in COVID-19 vaccine recipients. *Sci Immunol*. 2022;7(69):eabo2202.

33. Heitmann JS, Bilich T, Tandler C, et al. A COVID-19 peptide vaccine for the induction of SARS-CoV-2 T cell immunity. *Nature*. 2022;601(7894):617-622.

34. Li S, Jiang L, Li X, et al. Clinical and pathological investigation of patients with severe COVID-19. *JCI Insight*. 2020;5(12):e138070.

35. Sturrock A, Zimmerman E, Helms M, Liou TG, Paine R, 3rd. Hypoxia induces expression of angiotensin-converting enzyme II in alveolar epithelial cells: implications for the pathogenesis of acute lung injury in COVID-19. *Physiol Rep*. 2021;9(9):e14854.

36. Sturrock A, Woller D, Freeman A, Sanders K, Paine R, 3rd. Consequences of hypoxia for the pulmonary alveolar epithelial cell innate immune response. *J Immunol*. 2018;201(11):3411-3420.

37. Barilli A, Visigalli R, Ferrari F, Bianchi MG, Dall'Asta V, Rotoli BM. Immune-Mediated inflammatory responses of alveolar epithelial cells: implications for COVID-19 lung pathology. *Biomedicines*. 2022;10(3):618.

38. Varga Z, Flammer AJ, Steiger P, et al. Endothelial cell infection and endotheliitis in COVID-19. *Lancet*. 2020;395(10234):1417-1418.

39. Chua RL, Lukassen S, Trump S, et al. COVID-19 severity correlates with airway epithelium-immune cell interactions identified by single-cell analysis. *Nat Biotechnol*. 2020;38(8):970-979.

40. Hou Y, Zhou Y, Gack MU, et al. Multimodal single-cell omics analysis identifies epithelium-immune cell interactions and immune vulnerability associated with sex differences in COVID-19. *Signal Transduct Target Ther*. 2021;6(1):292.

41. Caforio ALP. Receipt of mRNA vaccine against Covid-19 and myocarditis. *N Engl J Med*. 2021;385(23):2189-2190.

42. Chey SW, Westerhoff M, Chey WD. Transient lymphocytic colitis after SARS-CoV2 mRNA vaccine. *Am J Gastroenterol*. 2022;117(4): 685-687.

43. Faissner S, Richter D, Ceylan U, Schneider-Gold C, Gold R. COVID-19 mRNA vaccine induced rhabdomyolysis and fasciitis. *J Neurol*. 2022;269(4):1774-1775.

SUPPORTING INFORMATION

Additional supporting information can be found online in the Supporting Information section at the end of this article.